AIAA JOURNAL
Vol. 30, No. 5, May 1992

Importance of Coatings to Optical Fiber Sensors Embedded in "Smart" Structures

Abhijit Dasgupta* and James S. Sirkis*
University of Maryland, College Park, Maryland 20743

The importance of coatings to the overall performance of optical fiber sensors embedded in "smart" host materials is explored with closed-form solutions. Particular attention is paid to the mechanical ramifications of varying the properties and thickness of the coating, when the fiber is embedded in a transversely isotropic host material that is experiencing tensile loading parallel to the optical fiber. Analytical solutions are developed that show that strain concentrations near an embedded optical fiber are highly dependent on the thickness and material properties of the coating. Analytical evidence is presented of the existence of optimum coating material and thickness combinations for a given host material. Depending on the optimizing criterion selected, this optimum choice can minimize or even eliminate stress concentrations either in the host material immediately surrounding the embedded fiber, or in the coating, or in the optical fiber itself.

Nomenclature

A,B	= unknown constants determined from boundary conditions
a,b	= radius of fiber and coating, respectively
C_{ij}	= material stiffness tensor, $i = 1$–6, $j = 1$–6
E	= Young's modulus
G	= shear modulus
r,z,θ	= orthonormal basis for cylindrical polar coordinate frame
u	= displacement
∂	= partial differential operator
ν	= Poisson's ratio
σ, ϵ	= stress and strain, respectively

Subscripts and Superscripts

c	= coating
f	= fiber
h	= host

Subscripts

ij	= Cartesian components of tensor quantity
LL,LT,TT	= stiffness components along material principal directions
r,z,θ	= cylindrical polar components along material principal directions
$rr,zz,\theta\theta$	= cylindrical polar components of tensor field quantity

Superscript

0	= applied far-field loading

I. Introduction

RESEARCH in intelligent structures is an area that integrates both mechanics and instrumentation. The smart structures concept is one where composite or monolithic load-bearing structures have embedded within them sensing and actuation instrumentation so that the structure can sense and respond automatically to environmental perturbations. Early research concentrated mostly on developing the sensors and actuators. Recently it has become recognized that mechanical issues cannot be ignored in the design of embeddable instrumentation. The possibility of perturbing the local strain field and of premature failing as a result of the embedded instrumentation must therefore be considered in the design process.

Czarnek et al.[1] used moiré interferometry, and Salehi et al.[2] used both moiré interferometry and finite element analysis to establish the existence of significant strain concentrations in the neighborhood of an optical fiber embedded in a laminated composite. Mathews and Sirkis[3] used hybrid stress analysis to establish lower, but still significant, strain concentrations in homogeneous isotropic hosts.

All of the studies just cited treated the embedded optical fiber as a single-phase component. This paper follows early optical fiber hydrophone[4] work by treating the optical fiber as a multiphase entity. As with optical fiber hydrophones, including the coating in the analysis provides additional degrees of freedom in the design process. In a real sense, the only direct influence that a designer can have on the mechanical issues of embedded optical fiber sensors is through sensor placement or through fiber coatings since the host structure and optical fiber properties are either specified or beyond the control of the sensor designer.

Coating parameters have been controlled by other investigators to influence damage properties of brittle materials,[5] temperature resistance,[6,7] interface bonding,[7,8] and phase sensitivity[8] characteristics of embedded optical fiber sensors. This paper explores the possibility of controlling coating parameters to minimize detrimental stress concentrations reported in the sensor assembly and in the surrounding host.[1-3] Evidence is presented that supports the existence of a mechanically "optimal" coating for the embedded optical fiber sensor. The term optimal is used in the sense that the stress state generated in the sensor assembly (fiber, coating, and surrounding host material) by the embedded optical fiber is least likely to produce conditions conducive to brittle failure and/or fatigue failure mechanisms at either the fiber-coating interface or the coating-host interface. Of these optimal criteria, only two specific cases have been considered in an earlier paper,[9] and a more generalized treatment is presented in this paper.

The optimization criteria are chosen from damage mechanics rationale as well as from the perspective of improving the accuracy of the strain sensor. Regions of high tensile stresses around the sensor assembly can promote nucleation of fatigue cracks and propagation of pre-existing flaws introduced by thermal expansion mismatches during the fabrication process. Hence, coatings that produce a zero or fully compressive stress state in or near the embedded sensor assembly are desirable. Further, since the optical fiber is typically calibrated under a

Received Oct. 16, 1990; revision received July 28, 1991; accepted for publication Aug. 18, 1991.

*Assistant Professor, Department of Mechanical Engineering.

state of zero transverse stresses, sensing accuracy is highest if the in situ tranverse normal stresses in the fiber, under external loads, can be eliminated by proper coating design. As will be illustrated in this paper, it is not always possible to satisfy all of the optimization criteria simultaneously, and the designer may have to prioritize the conflicting criteria and perform design tradeoffs, depending on the specific needs. However, this paper presents all of the necessary analytical background and illustrates the methodology for creating the necessary design tools.

When defining the optimization criteria in this paper, it is assumed as a first-order approximation, that the residual stress state in the neighborhood of the sensor assembly due to fabrication process is negligible. It is further assumed that perfect bonding exists at the interfaces between the optical fiber, coating, and host and that no chemical interactions occur. Although the limitations of such assumptions are recognized, it is pointed out that the aim here is merely to illustrate that the coating properties and geometry do influence the stress state in the sensor assembly and that their investigation is both worthwhile and beneficial.

The sensor assembly is considered to be embedded in a transversely isotropic composite host. Stress states due to external loading are then explored for varying combinations of the coating's Young's modulus and Poisson's ratio. For convenience, a design space is defined where the variables are the coating diameter and the two independent stiffness constants for an isotropic coating material. The analytical treatment of the stress state surrounding the embedded optical fiber shows the existence of optimal curves in this coating design space, when different transverse normal stress components (hoop or radial) in different phases (fiber, coating, or host) of the sensor assembly are targeted for minimization (or, in the absence of residual stresses, for elimination). The Poisson's ratio, Young's modulus, and diameter of the coating along these optimal curves define the optimal coating.

II. Optical Fiber Embedded in a Transversely Isotropic Host Material

The phase sensitivity of a structurally embedded interferometric optical fiber sensor is dominated by the normal strain component that is everywhere tangent to the fiber axis.[10] It is therefore most appropriate first to examine the mechanical role of the optical fiber coating when the host structure is subjected to uniform normal strain, parallel to the optical fiber axis.

For the purpose of this analysis, the host material is assumed to be transversely isotropic with the fiber axis being normal to the plane of isotropy. Such situations arise, for example, when the optical fiber is embedded in a fiber-reinforced composite material whose native reinforcing fibers are aligned parallel to the optical fiber. When the composite fibers are not parallel to the optical fiber, one observes lenticular resin pockets around the optical fiber. Such a geometric configuration is inappropriate for the solution technique proposed here and is addressed elsewhere in the literature.[1,2,11] An optical fiber embedded in an isotropic host is a degenerate of the transversely isotropic case, and the solutions presented in this paper are equally applicable, provided that the material properties of the host are properly defined.

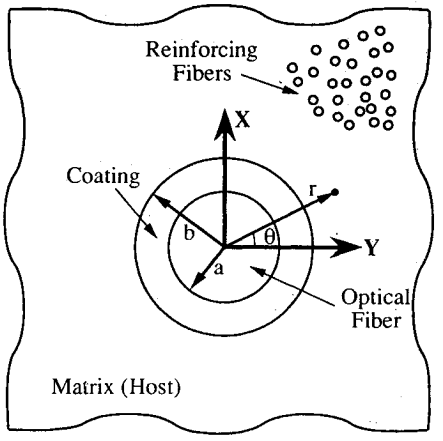

Fig. 1 Schematic of coated optical fiber embedded in a fiber-composite host.

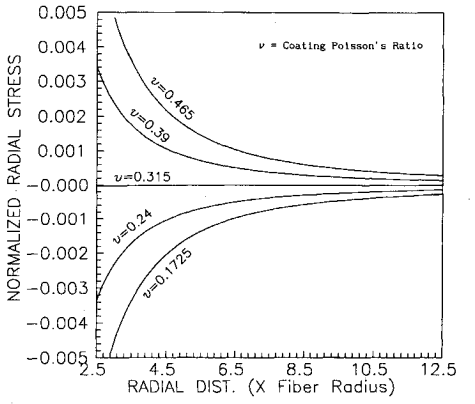

Fig. 2a Normalized radial stress distribution in host for coatings with $E = 147$ GPa and five different Poisson's ratios (x axis normalized with respect to fiber radius and shown from the coating-host interface outwards).

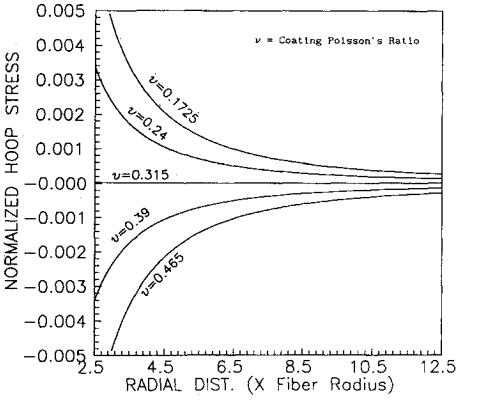

Fig. 2b Normalized hoop stress distribution in host for coatings with $E = 147$ GPa and five different Poisson's ratios (x axis normalized with respect to fiber radius and shown from the fiber-coating interface outwards).

The axisymmetric displacement field in this case is assumed in accordance with Lamé[12] for the geometry of Fig. 1 as

Fiber:

$$u_r^f = A_f r \tag{1a}$$

Coating:

$$u_r^c = A_c r + B_c/r \tag{1b}$$

Host:

$$u_r^h = A_h r + B_h/r \tag{1c}$$

and

$$u_z = \epsilon_{zz}^0 z, \qquad u_\theta = 0 \tag{1d}$$

for all three phases of the structure. In these equations, ϵ_{zz}^0 is the applied far-field axial strain, A_i and B_i $(i = f, c, h)$ are unknown constants to be determined from the appropriate

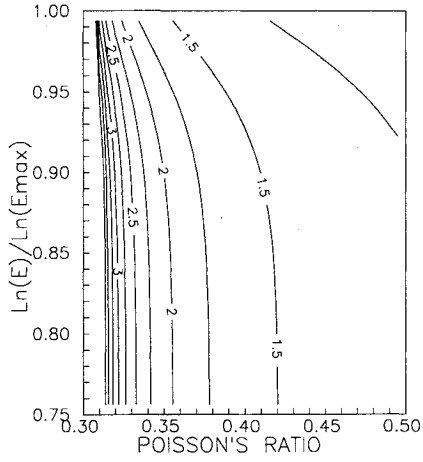

Fig. 3 Contours of optimum coating radius normalized with respect to fiber radius (b/a) shown in coating material design space, for eliminating transverse stresses in the host (the coating's Young's modulus E is normalized with respect to E_{max}, the Young's modulus of steel, ν is the Poisson's ratio of the coating).

boundary conditions, and r is the radial polar coordinate. The strains are found in polar coordinates (assuming small displacements) as

$$\epsilon_{rr} = \frac{\partial u_r}{\partial r} \tag{2a}$$

$$\epsilon_{\theta\theta} = \frac{u_r}{r} + \frac{1}{r}\frac{\partial u_\theta}{\partial \theta} \tag{2b}$$

$$\epsilon_{zz} = \epsilon_{zz}^0 \tag{2c}$$

The stresses in the optical fiber and the coating obey the isotropic Hooke's Law

$$\sigma_{rr}^{f,c} = C_{f,c}[(1-\nu_{f,c})\epsilon_{rr}^{f,c} + \nu_{f,c}(\epsilon_{\theta\theta}^{f,c} + \epsilon_{zz}^{f,c})] \tag{3a}$$

$$\sigma_{\theta\theta}^{f,c} = C_{f,c}[(1-\nu_{f,c})\epsilon_{\theta\theta}^{f,c} + \nu_{f,c}(\epsilon_{rr}^{f,c} + \epsilon_{zz}^{f,c})] \tag{3b}$$

where $C = E/(1+\nu)(1-2\nu)$. The stresses in the host obey the transversely isotropic Hooke's law

$$\sigma_{rr}^{h} = (C_{11}^{h}\epsilon_{rr}^{h} + C_{12}^{h}\epsilon_{\theta\theta}^{h} + C_{13}^{h}\epsilon_{zz}^{h}) \tag{4a}$$

$$\sigma_{\theta\theta}^{h} = (C_{12}^{h}\epsilon_{rr}^{h} + C_{11}^{h}\epsilon_{\theta\theta}^{h} + C_{13}^{h}\epsilon_{zz}^{h}) \tag{4b}$$

where stiffness coefficients C_{ij} are given explicitly in terms of the engineering constants in the Appendix. The constants A_i and B_i are computed by satisfying continuity of displacement and traction fields across the interfaces between the fiber, coating, and host. For the axisymmetric case under consideration here, these conditions apply to the radial displacement and stress components as stated next:

$$u_r^f(a) = u_r^c(a) \tag{5a}$$

$$u_r^c(b) = u_r^h(b) \tag{5b}$$

$$\sigma_{rr}^f(a) = \sigma_{rr}^c(a) \tag{5c}$$

$$\sigma_{rr}^c(b) = \sigma_{rr}^h(b) \tag{5d}$$

where, as shown in Fig. 1, a and b are the radii of the fiber-coating and coating-host interfaces, respectively.

Finally, a fifth boundary condition is imposed by requiring the far-field radial stress to vanish as r approaches ∞. Thus,

$$\lim_{r\to\infty}(\sigma_{rr}^h) = 0 \tag{5e}$$

The five constants A_i and B_i are obtained by satisfying the five equations (5a–5e), as provided in the Appendix. Once the unknown constants in the displacement field have been determined, the strain and stress fields can be uniquely determined in the fiber, coating, and host materials, as functions of radius.

As an example, a glass optical fiber of 80 μm diameter with a 200-μm-diam coating is embedded in a unidirectional graphite epoxy composite host. The glass fiber is isotropic and is characterized by $E = 69$ GPa and $\nu = 0.17$. The host is assumed to have 60% volume fraction of unidirectional graphite fibers in a room-temperature curable thermoset epoxy. The elastic properties of the composite are assumed as $E_L = 134.45$ GPa, $E_T = 10.2$ GPa, $\nu_{TT} = 0.49$, $\nu_{LT} = 0.30$, where subscripts L and T indicate directions longitudinal and transverse, respectively, to the reinforcing fibers of the composite host. Since the composite fibers are assumed to run parallel to the optical fiber in this analysis, the axis of the optical fiber (direction 3 or L) is normal to the plane of transverse isotropy (plane 12 or TT) of the host.

Analytical predictions of the radial and hoop stresses in this host are shown as a function of radius in Figs. 2a and 2b, respectively, for five selected coating materials, of Young's modulus 147 GPa and Poisson's ratios 0.1725, 0.24, 0.315, 0.39, and 0.465. It is noted that the magnitude and sign of the transverse (hoop and radial) stresses can be controlled by changing the coating properties. The hoop stress is positive at a Poisson's ratio of 0.1725 and decreases to negative values as the Poisson's ratio of the coating is increased, whereas the radial stress starts negative and becomes progressively positive as the Poisson's ratio is increased. Since the hoop and radial stresses, for the given displacement assumption, are equal in magnitude and of opposite sign everywhere in the host, both transverse stress components vanish simultaneously throughout the host for a particular choice of coating property. For the example presented here, this transition occurs when the Poisson's ratio of the coating is 0.315. This behavior suggests the existence of an optimum coating material for the given host and fiber material system and geometry and is significant in suggesting that the large stress (and strain) concentrations reported in Refs. 1–3 may be minimized (and, in the absence of residual stresses, completely eliminated) by judicious choice of coating material and/or coating diameter. This and other optimization criteria for coating design are considered in the following section.

III. Optimal Coatings

The existence of optimal coating choices for the configuration described earlier is now explored in terms of the three design parameters listed earlier, viz., the two independent material constants for the isotropic coating material and the geometry (thickness or b/a ratio) of the coating. Specifically, optimum geometries (b/a ratios) are computed for a wide choice of properties of the coating material. The results are presented in a design space defined by a coating's Young's modulus E_c ranging from 0.3 GPa (RTV silicone properties) to 200 GPa (steel properties) in equal increments on a log scale, and a coating's Poisson's ratio ν_c ranging from 0.1 to 0.5 uniformly on a linear scale. The Young's modulus is represented as a nondimensional ratio on a log scale to encompass a large range of values. Four different optimization criteria are possible for selecting the best geometry (b/a ratio) and each is discussed in detail in the following subsections.

A. Coatings for Eliminating Transverse Stresses in Host

It is important to minimize the possibility of generating fatigue and overstress cracks at the coating-host interface, which may then propagate through the host material, thus compromising structural integrity. Since, in the absence of residual stresses, it is not possible to generate compressive values for both transverse stress components simultaneously

Table 1 Sign of nonzero stresses for each optimal condition

Stress terms eliminated	Stress terms affected			
	$\sigma^f_{\theta\theta}$ (and $-\sigma^f_{rr}$)	$\sigma^c_{\theta\theta}$ (at $r=a$)	$\sigma^c_{\theta\theta}$ (at $r=b$)	$\sigma^h_{\theta\theta}$ (and $-\sigma^h_{rr}$) (at $r=b$)
$\sigma^h_{\theta\theta}$ (and $-\sigma^h_{rr}$)	negative	positive	positive	zero
$\sigma^f_{\theta\theta}$ (and $-\sigma^f_{rr}$)	zero	positive	positive	negative
$\sigma^c_{\theta\theta}$ (at $r=a$)	negative	zero	negative	positive
$\sigma^c_{\theta\theta}$ (at $r=b$)	negative	positive	zero	positive

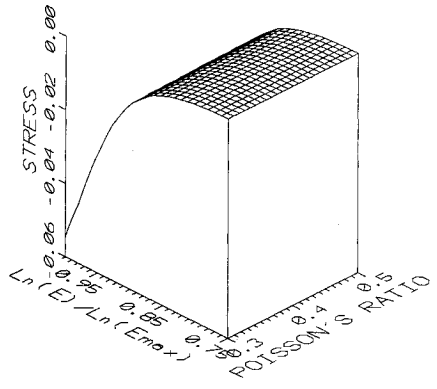

Fig. 4a Transverse stresses in the fiber when transverse stresses in host are eliminated.

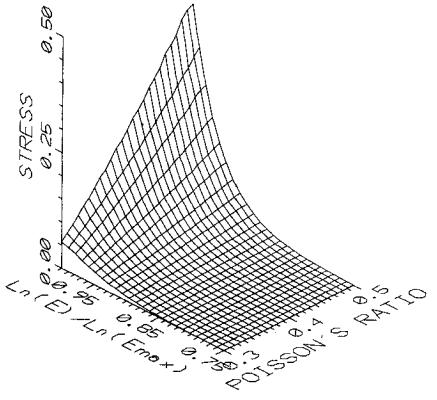

Fig. 4b Hoop stress in coating at fiber-coating interface when transverse stresses in host are eliminated.

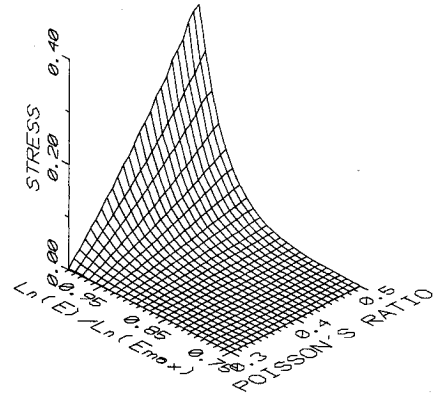

Fig. 4c Hoop stress in coating at fiber-coating interface when transverse stresses in host are eliminated.

in the host, zero stresses obviously represent the only real optimum choice. An analytical expression defining the optimum conditions for zero transverse matrix stresses can be found by forcing the radial and hoop stresses in the transversely isotropic Hooke's Law [Eqs. (4a) and (4b)] to zero. The resulting condition is that a biaxial state of strain ($\epsilon^h_{rr} = \epsilon^h_{\theta\theta}$) must exist throughout the host. By using the axisymmetric strain-displacement relations [Eqs. (2)], the biaxial strain condition becomes

$$\frac{\partial u_r}{\partial r} = \frac{u_r}{r} \tag{6}$$

which, as seen from Eq. (1), can only be satisfied if B_h equals zero. Setting B_h to zero in Eq. (A6) in the Appendix, one obtains the required condition of optimal coatings as

$$\frac{(2G_c + C_f)(\nu_c - \nu^h_{31})}{2(1-\nu_c)} = \frac{C_f(\nu_f - \nu^h_{31})}{[1-(b/a)^2]} \tag{7}$$

where ν^h_{31} is the longitudinal major Poisson's ratio ν_{LT} of the transversely isotropic composite host.

Equation (7) illustrates the fact that the optimum combination of coating material and diameter varies only with the host Poisson's ratio and is independent of the host stiffness. Thus, two different host materials with the same Poisson's ratio would still have the same optimal choice of coating configuration. Equation (7) is illustrated graphically in Fig. 3 where optimal (b/a) ratios are presented as a contour plot in the coating material design space for the graphite epoxy composite host described earlier. The ν_c axis here spans only from 0.3 to 0.5 since there are no admissible solutions to Eq. (6) for coatings with $\nu_c < \nu^h_{31}$. This subset is termed the reduced coating material design space for the remainder of this paper, and all subsequent results are presented in this reduced design space for convenience. This graph constitutes an important design tool since for any given combination of E_c and ν_c the designer can choose an optimum (b/a) value. Clearly, in view of Eq. (6), this plot is equally valid for all other host materials with a major longitudinal Poisson's ratio ν^h_{31} of 0.30.

Table 1 summarizes the sign of the nonzero transverse stresses elsewhere in the sensor assembly when the coating is optimized to eliminate the transverse stresses in the host. Compressive stresses are generally considered to be beneficial and are preferred to detrimental tensile stresses. Corresponding distribution of transverse stresses in the fiber and coating are shown in Figs. 4a–4c for an optimal coating, where the results are presented in the reduced coating material design space with stresses shown on the vertical axis. All stresses are nondimensionalized by the normalizing factor $E^h_{33}\epsilon^0_{zz}$. Transverse stresses σ_{rr} and $\sigma_{\theta\theta}$ in the fiber (which are, by definition, equal to each other and uniform) are shown in Fig. 4a. These stresses are relatively insensitive to the coating Poisson's ratio and take increasingly compressive values as the coating stiffness is increased. Figures 4b and 4c show the hoop stresses in the coating at the fiber-coating and coating-host interfaces, respectively. (Hoop stresses in the fiber and host at their respective interfaces with the coating are equal in magnitude —though of opposite sign in the host—to the respective radial

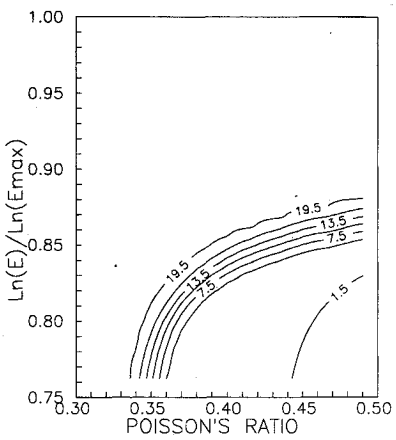

Fig. 5 Contours of optimum coating radius normalized with respect to fiber radius (b/a) shown in coating material design space, for eliminating transverse stresses in the fiber (the coating's Young's modulus E is normalized with respect to E_{max}, the Young's modulus of steel; ν is the Poisson's ratio of the coating).

stresses and hence are not displayed in any of the discussions in this paper.) Clearly, the coating hoop stresses increase with both stiffness and Poisson's ratio of the coating. It should be noted that large positive hoop stresses are detrimental from the perspective of generating radial cracks at the interfaces. Transverse stresses in the host are, by definition, zero valued and therefore are not displayed.

B. Coatings for Eliminating Transverse Stresses in the Fiber

The transverse stresses in the fiber are also of interest. Eliminating the transverse stresses in the fiber not only lowers the probability of initiating damage in the fiber or at the fiber-coating interface but also brings the in situ strain state on the fiber closer to the strain state under which it was originally calibrated.[13] This ensures higher sensing accuracy and higher reliability of the sensor as a whole. To this end, one can develop relations similar to Eq. (7) to eliminate transverse stresses in the fiber. By definition, the radial stress in the coating at the fiber-coating interface is also simultaneously eliminated. Setting the fiber stresses in Eq. (3) to zero yields the constraint condition as

$$A_f = -\nu_f \epsilon^0_{zz} \tag{8}$$

where A_f is given by Eq. (A3). It can be readily shown that Eq. (8) leads to the constraint condition

$$(b/a)^2\{(\nu_c-\nu_f)[(1-2\nu_c)C_c-2G^h_{12}]+4G^h_{12}(\nu^h_{31}-\nu_f)(1-\nu_c)\}$$

$$+2(\nu_c-\nu_f)(G^h_{12}-G_c)=0 \tag{9}$$

where G^h_{12} is the transverse shear stiffness of the composite host. Since the transverse plane is the plane of isotropy,

$$G^h_{12}=E^h_{11}/[2(1+\nu^h_{12})]=E^h_{TT}/[2(1+\nu^h_{TT})]$$

As was observed when eliminating host stresses, the optimal condition depends only on the Poisson's ratio and not on the stiffness of the phase in which the transverse stresses are being eliminated. Although Eq. (9) has admissible solutions for $\nu_c < \nu^h_{13}$, the results display a discontinuity at ν^h_{13}. Therefore, for convenience and brevity of presentation, the results are displayed in Fig. 5 in the reduced coating material design space discussed earlier in Sec. III.A. Figure 5 illustrates that admissible solutions in the present case are possible only over a subset of the reduced coating material design space. Figures 3 and 5 also illustrate that Eqs. (6) and (9) do not have any common solutions, as evidenced by the fact that constant (b/a) lines do not intersect. Thus both optimization criteria cannot be satisfied simultaneously, and design tradeoffs are necessary.

The nonzero stresses for this optimization criterion can be computed as in Sec. III.A. The signs of these stresses are summarized in Table 1, but detailed stress information is not presented here for reasons of brevity.

C. Coatings Without Hoop Stresses at Interfaces

The coating radial stresses at the interfaces are automatically eliminated, by virtue of traction continuity, in cases described in Secs. III.A and III.B. However, the same is not true for the hoop stresses. Eliminating the hoop stresses may become an important factor from radial crack propagation considerations, if the coating is a relatively brittle material such as the carbon coatings used for hermiticity. In this section, equations are presented for eliminating hoop stresses in the coating at the fiber-coating and coating-host interfaces, respectively. The nonzero stresses for these optimization criteria are summarized in Table 1, and detailed information is omitted in this paper for reasons of brevity.

1. Fiber-Coating Interface

It can be readily demonstrated, by substituting Eqs. (A1–A11) in Eq. (4b) and setting $\sigma_{\theta\theta}$ to zero, that the hoop stresses in the coating at $r=a$ (fiber-coating interface) disappear identically when the coating geometry (b/a ratio) and coating properties satisfy the following constraint:

$$(b/a)^2(C_c+2G^h_{12})\,[(2G_c+C_f)Q-(1-2\nu_c)P]$$
$$=2[(C_f-C_c)Q-P]\,(G_c-G^h_{12}) \tag{10}$$

where

$$P=(C_c-2G^h_{12})(C_c\nu_c-C_f\nu_f)+(C_f-C_c)(C_c\nu_c+2G^h_{12}\nu^h_{31})$$

$$Q=2G^h_{12}\,(\nu^h_{31}-\nu_c)$$

Unlike Eqs. (7) and (9), constraint equation (10) is not independent of the stiffness of the phase where the stress is being eliminated. As in Eq. (9), this condition on the coating material choice is observed to be more restrictive than Eq. (7) since only a limited portion of the design space actually contains admissible solutions. This fact is illustrated in Fig. 6 for the same reduced design space used in Figs. 3 and 5. Unfortunately, Eq. (10) does not have any solutions in common with either Eq. (7) or (9). Therefore, it is not possible to eliminate coating hoop stresses at this interface while simultaneously

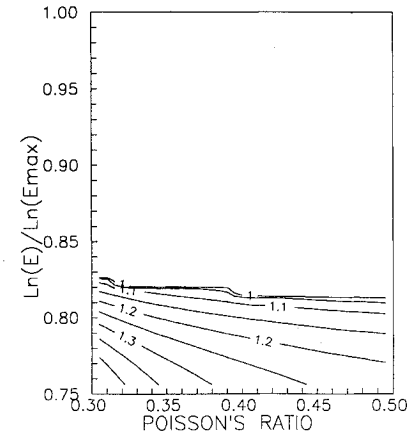

Fig. 6 Contours of optimum coating radius normalized with respect to fiber radius (b/a) shown in coating material design space, for eliminating coating hoop stresses at fiber-coating interface, $r=a$ (the coating's Young's modulus E is normalized with respect to E_{max}, the Young's modulus of steel; ν is the Poisson's ratio of the coating).

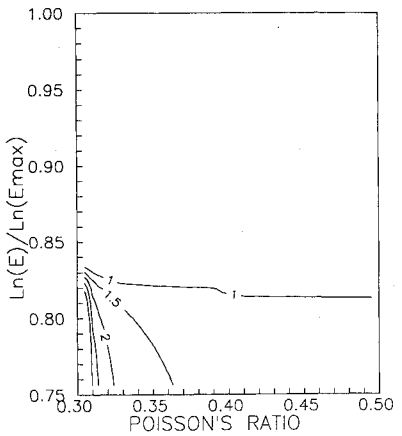

Fig. 7 Contours of optimum coating radius normalized with respect to fiber radius (b/a) shown in coating material design space, for eliminating coating hoop stresses at coating host interface, $r=b$ (the coating's Young's modulus E is normalized with respect to E_{max}, the Young's modulus of steel; ν is the Poisson's ratio of the coating).

eliminating transverse stresses either in the fiber or in the host for any real choice of coating material or coating diameter. However, as discussed in Sec. III.B, the information presented in Fig. 6 is useful for design tradeoffs when used in conjunction with Figs. 3 and 5. The kinks observed in the contours in the neighborhood of $b/a=1$ are due to a computational inadequacy of the gridding and interpolation algorithm in the graphics software that causes a quantum jump from one grid row to the next whenever the contour has a small angle of inclination to the horizontal axis.

2. Coating-Host Interface

The constraint condition at $r=b$ is very similar to Eq. (10) derived in Sec. III.C.1 and can be shown to be

$$(C_c+2G_{12}^h)\,[(b/a)^2\,(2G_c+C_f)\,Q-(1-2\nu_c)\,P]$$
$$=2\,[(C_f-C_c)Q-P]\,(G_c-G_{12}^h) \tag{11}$$

where P and Q are defined in Eq. (10).

Figure 7 shows a plot of Eq. (11) in the reduced design space and illustrates the fact that only a limited portion of the design space contains admissible solutions. Again, there are no solutions in common with any of Eqs. (7), (9), or (10). However, Figs. 3 and 5–7 together constitute a complete set of design tools required for tailoring the stress field in the sensor assembly, as per the designer's requirements. As in Fig. 6, the kinks observed in some of the contour lines in Fig. 7 are also numerical artifacts of the graphics software, due to limitations discussed in Sec. III.C.1.

IV. Conclusion

Valuable design information for smart structures has been presented by examining the analytical description of the stress and strain state surrounding a coated optical fiber sensor embedded in a transversely isotropic laminated composite host material. The most important conclusion of this analysis is that the transverse stresses σ_{rr} and $\sigma_{\theta\theta}$ in the fiber, coating, and host can be tailored to the designer's requirements by changing the material and/or geometry of the coating. In fact, in the absence of residual stresses, certain combinations of coating materials and radius can cause the transverse stress components σ_{rr} and $\sigma_{\theta\theta}$ to become identically zero, under tensile loading parallel to the optical fiber, thereby raising the prospect of designing optimal coatings for smart structure sensors.

Closed-form expressions are derived for four different optimal situations by eliminating different transverse stresses in different phases of the sensor assembly at the two different interfaces. As an illustrative example, quantitative results are presented for a glass optical fiber embedded in a unidirectional graphite epoxy composite host. Results indicate that solutions to the constraint equations for the four optimal situations are mutually exclusive for this material system. Table 1 summarizes the results and indicates the sign of the remaining nonzero transverse stresses for each of the four cases examined. This table is useful when conducting design tradeoff studies since it tells the designer at a glance when and where beneficial (compressive) transverse stresses may be expected. For more detailed information such as sensitivity of the stresses to coating parameters, figures such as the ones presented in Sec.III.A are necessary.

The results presented in this paper are specific to this material system and to the case of uniform axial loading parallel to the optical fiber. However, the importance of the results lie in their demonstration that the coating choice has a significant impact on the mechanics and performance of embedded optical fiber sensors. Hence, coatings should be carefully considered during smart structure design.

Appendix

The system of equations produced by applying the boundary conditions specified in Eqs. (5) can be immediately reduced to a four-by-four system by first directly solving Eq. (5e) to yield

$$A_h = -\bar{A}_h\epsilon_{zz}^0$$

where

$$\bar{A}_h=\frac{C_{13}^h}{C_{11}^h+C_{12}^h}=\nu_{31}^h \tag{A1}$$

Conditions (5a–5d) then yield

$$\begin{bmatrix} a^2 & -a^2 & -1 & 0 \\ a^2C_f & -a^2C_c & 2G_c & 0 \\ 0 & b^2 & 1 & -1 \\ 0 & b^2C_c & -2G_c & (C_{11}^h-C_{12}^h) \end{bmatrix} \begin{bmatrix} A_f \\ A_c \\ B_c \\ B_h \end{bmatrix}$$
$$= \begin{bmatrix} 0 \\ a^2(C_c\nu_c-C_f\nu_f)\epsilon_{zz}^0 \\ -b^2\bar{A}_h\epsilon_{zz}^0 \\ -b^2\nu_cC_c\epsilon_{zz}^0 \end{bmatrix} \tag{A2}$$

Solving system (A2) with Cramer's rule, the unknown constants are

$$A_f=\frac{b^2[(C_{11}^h-C_{12}^h)\bar{A}_h+\nu_cC_c](2G_c+C_c)\epsilon_{zz}^0}{\text{Det }[M]}$$
$$-\frac{b^2(C_{11}^h-C_{12}^h+C_c)(C_c\nu_c-C_f\nu_f)\epsilon_{zz}^0}{\text{Det }[M]}$$
$$+\frac{a^2(C_{11}^h-C_{12}^h-2G_c)(C_c\nu_c-C_f\nu_f)\epsilon_{zz}^0}{\text{Det }[M]} \tag{A3}$$

$$A_c=\frac{a^2(C_{11}^h-C_{12}^h-2G_c)(C_c\nu_c-C_f\nu_f)\epsilon_{zz}^0}{\text{Det }[M]}$$
$$+\frac{b^2[(C_{11}^h-C_{12}^h)\bar{A}_h+\nu_cC_c](2G_c+C_f)\epsilon_{zz}^0}{\text{Det }[M]} \tag{A4}$$

$$B_c=-\frac{a^2b^2(C_{11}^h-C_{12}^h+C_c)(C_c\nu_c-C_f\nu_f)\epsilon_{zz}^0}{\text{Det }[M]}$$
$$-\frac{a^2b^2[(C_{11}^h-C_{12}^h)\bar{A}_h+\nu_cC_c](C_f-C_c)\epsilon_{zz}^0}{\text{Det }[M]} \tag{A5}$$

$$B_h = -\frac{a^2b^2(2G_c + C_c)(C_c\nu_c - C_f\nu_f)\epsilon_{zz}^0}{\text{Det } [M]}$$

$$-\frac{b^2[b^2(2G_c + C_f)C_c + 2a^2G_c(C_f - C_c)\bar{A}_h]\epsilon_{zz}^0}{\text{Det } [M]}$$

$$-\frac{b^2[a^2(C_f - C_c) - b^2(2G_c + C_f)]C_c\nu_c\epsilon_{zz}^0}{\text{Det } [M]} \quad \text{(A6)}$$

where

$$\text{Det } [M] = a^2(C_f - C_c)(2G_{12}^h - 2G_c) - b^2(2G_c + C_f)(2G_{12}^h + C_c) \quad \text{(A7)}$$

The previous equations also hold for isotropic host materials, since for isotropic materials $C_{11}^h - C_{12}^h = 2G_h$ and $\bar{A}_h = \nu_h$. The transversely isotropic stiffness constants C_{11}^h, C_{12}^h, and C_{13}^h used in Sec. III and in the previous equations for the host material are obtained explicitly from the engineering stiffness constants of the material as follows:

$$C_{11}^h = C^h(E_{33}^h/E_{11}^h - \nu_{31}^{h2}) \quad \text{(A8)}$$

$$C_{12}^h = C^h(E_{33}^h\nu_{12}^h/E_{11}^h + \nu_{31}^{h2}) \quad \text{(A9)}$$

$$C_{13}^h = C^hE_{33}^h\nu_{31}^h\ (1 + \nu_{12}^h)/E_{11}^h \quad \text{(A10)}$$

where

$$C^h = E_{11}^h/\{(1 + \nu_{12}^h)[E_{33}^h(1 - \nu_{12}^h)/E_{11}^h - 2\nu_{31}^h]\} \quad \text{(A11)}$$

The directions 1 and 2 lie in the plane of transverse isotropy, and direction 3 is along the optical fiber axis.

Acknowledgment

This work was partially supported by the National Science Foundation under Grant ECS-8914865.

References

[1]Czarnek, R., Guo, Y. F., Bennet, K. D., and Claus, R. O., "Interferometric Measurements of Strain Concentrations Induced by an Optical Fiber Embedded in a Fiber Reinforced Composite," *Fiber Optic Smart Structures and Skins I*, Vol. 986, Society of Photo-Optical Instrumentation Engineers, Bellingham, WA, 1988, pp. 120–129.

[2]Salehi, A., Tay, A., Wilson, D., and Smith, D., "Strain Concentrations Around Embedded Optical Fibers by FEM and Moiré Interferometry," *Proceedings of the 5th Annual ASM/ESD Advanced Composites Conference/Exposition*, ASM International, Materials Park, OH, 1989, pp. 11–19.

[3]Mathews, C. T., and Sirkis, J. S., "The Interaction Mechanics of Interferometric Optical Fiber Sensors Embedded in a Monolithic Structure," *Fiber Optic Smart Structures and Skins III*, Vol. 1370, Society of Photo-Optical Instrumentation, San Jose, CA, 1990, pp. 142–153.

[4]Giallorenzi, T., Bucaro, J., Dandridge, A., Siegal, G., Cole, J., Raleigh, S., and Priest, R., "Optical Fiber Sensing Technology," *IEEE Journal of Quantum Electronics*, Vol. QE-8, No. 4, 1982, pp. 626–665.

[5]Sigl, L. S., and Evans, A. G., "Effects of Residual Stress ;and Frictional Sliding on Cracking and Pull-Out in Brittle Matrix Composites," *Mechanics of Materials*, Vol. 8, No. 1, 1989, pp. 1–12.

[6]Urruti, E. H., and Wahl, J. F., "Coatings Affect Fiber Performance in Smart-Skin Sensing," *Laser Focus World*, Vol. 26, No. 1, 1990, pp. 165–169.

[7]DiFrancia, C., and Claus, R., "Structure/Property Correlations of Several Polyimide Optical Fiber Coatings for Embedding in an Epoxy Matrix," *Fiber Optic Smart Structures and Skins II*, Vol. 1170, Society of Photo-Optical Instrumentation Engineers, Bellingham, WA, 1989, pp. 505–512.

[8]Lagakos, N., Bucaro, J. A., Ehrenfeuchter, P., Hickman, T. R., Tveten, A. B., and Dandridge, A., "Planar-Conformal Fiber Optic Acoustic Sensing Elements," *Fiber Optic Smart Structures and Skins II*, Vol. 1170, Society of Photo-Optical Instrumentation Engineers, Bellingham, WA, 1989, pp. 473–477.

[9]Dasgupta, A., and Sirkis, J. S., "The Importance of Coatings to Structurally Embedded Optical Sensors," *Proceedings of the ISA 90 International Conference*, Instrument Society of America, Research Triangle Park, NC, 1990, pp. 1673–1693.

[10]Sirkis, J. S., and Haslach, H. W., "Full Phase-Stain Relation for Structurally Embedded Interferometric Optical Fiber Sensors," *Fiber Optic Smart Structures and Skins III*, Vol. 1370, San Jose, CA, 1990, pp. 248–259.

[11]Dasgupta, A., Wan, Y., Sirkis, J. S., and Singh, H., "Experimental and Numerical Micro-Mechanical Investigation of an Optical Fiber Embedded in a Laminated Composite," *Fiber Optic Smart Structures and Skins III*, Vol. 1370, Society of Photo-Optical Instrumentation Engineers, San Jose, CA, 1990, pp. 119–128.

[12]Lamé, G., *Lecons sur la Theorie Mathematique de l'elaticite' des Corps Solides*, Bachelier, Paris, 1852.

[13]Sirkis, J. S., and Haslach, H. W., "Interferometric Strain Measurement by Arbitrarily Configured, Surface Mounted, Optical Fibers," *Journal of Lightwave Technology*, Vol. 8, No. 10, 1990, pp. 1497–1503.